Versão do arquivo anexado / Version of attached file:

Versão do Editor / Published Version

Mais informações no site da editora / Further information on publisher's website:

https://www.nature.com/articles/s41598-017-19066-3

DOI: 10.1038/s41598-017-19066-3

Direitos autorais / Publisher's copyright statement:

SCIENTIFIC REP⬛RTS

Engineered nonlinear materials using gold nanoantenna array

Vladimir P. Drachev[1,2], Alexander V. Kildishev[3], Joshua D. Borneman[3], Kuo-Ping Chen[3], Vladimir M. Shalaev[3], Konstantin Yamnitskiy[4], Robert A. Norwood[4], Nasser Peyghambarian[4], Seth R. Marder[5], Lazaro A. Padilha[6,8], Scott Webster[6], Trenton R. Ensley[6,9], David J. Hagan[6,7] & Eric W. Van Stryland[6,7]

Gold dipole nanoantennas embedded in an organic molecular film provide strong local electromagnetic fields to enhance both the nonlinear refractive index (n_2) and two-photon absorption (2PA) of the molecules. An enhancement of 53× for 2PA and 140× for nonlinear refraction is observed for BDPAS (4,4′-bis(diphenylamino)stilbene) at 600 nm with only 3.7% of gold volume fraction. The complex value of the third-order susceptibility enhancement results in a sign change of n_2 for the effective composite material relative to the pure BDPAS film. This complex nature of the enhancement and the tunability of the nanoantenna resonance allow for engineering the effective nonlinear response of the composite film.

Nanoantennas have gathered great attention due to their strong, frequency tunable, electromagnetic field enhancement[1]. These large local fields enable many applications in near-field optics, nonlinear optics[2], and fluorescence research[3,4]. Although plasmonic nanoparticles have been employed to enhance nonlinear absorption[5,6], two-photon absorption (2PA) enhancement in those cases was mainly detected using two-photon excited luminescence, which is not the same as obtaining observable nonlinear absorption in transmission for the composite material[7,8]. This is because transmission measurements include contributions from both the loss due to the metal nanoparticles and the enhanced absorption of the molecules. Furthermore, the field enhancement is a complex quantity, which cross-couples nonlinear absorption and refraction.

Note, that nonlinear response enhancement due to the intrinsic nonlinearity of plasmonic nanoantennas has previously been explored in some detail but still attracts great interest. These include studies on nanoparticle size-dependence of the nonlinear response[9–13], from atomic clusters to plasmonic nanocrystals of Ag and Au[14–17], optical Kerr-effect, inverse Faraday effect and nonlinear optical activity for metal nanoparticles and aggregates[18,19], enhancing nonlinearity by using metasurfaces and metamaterial structures[20], theory on figure-of-merit for nonlinear response[21], core-shell for enhanced second-harmonic[22], metasurface defined with e-beam lithography of α-Si:H nanorods for ultrafast spectral and polarization switching[23].

However, the enhancement of the "external" material nonlinearity caused by nanoantennas is less well studied. This paper considers nanoantentennas as a pair of nanoparticles, which allows tunability of the plasmon resonance by changing the particle geometry and/or gap size. The nanoantenna array quality requires e-beam lithography defined fabrication and the ability to resist laser damage at high powers.

The effective third-order susceptibility of a metal dielectric composite, in the simplest case[24,25], is a product of two complex values: the enhancement factor and the third-order susceptibility of the component materials, which are both wavelength dependent. Therefore, one can engineer an effective nonlinear material by matching the nanoantenna resonance and the wavelength dependence of the susceptibility.

In this paper we describe the use of a gold nanoantenna array to enhance both the nonlinear refractive index (n_2) and 2PA of the organic dye 4,4′-bis(diphenylamino)stilbene (BDPAS), which is known as a dye with relatively large 2PA[26–28]. Experimental results show a 53× enhancement for the effective nonlinear absorption, α_2, of the composite layer at 600 nm, as supported by 3D finite element method (FEM) numerical simulations. The

[1]Department of Physics and Advanced Materials & Manufacturing Institute, University of North Texas, Denton, Texas 76203, USA. [2]Skolkovo Institute of Science and Technology, Moscow 143026, Russia. [3]School of Electrical and Computer Engineering and Birck Nanotechnology Center, Purdue University, West Lafayette, IN 47907, USA. [4]College of Optical Sciences, University of Arizona, Tucson, AZ 85721, USA. [5]Georgia Institute of Technology, Atlanta, GA 30332, USA. [6]CREOL, The College of Optics and Photonics, University of Central Florida, Orlando, FL 32816, USA. [7]Department of Physics, University of Central Florida, Orlando, FL 32816, USA. [8]Present address: Univ Estadual Campinas, UNICAMP, Sao Paulo, Brazil. [9]Present address: U.S. Army Research Laboratory, Adelphi, MD 20783, USA. Correspondence and requests for materials should be addressed to V.P.D. (email: vladimir.drachev@unt.edu)
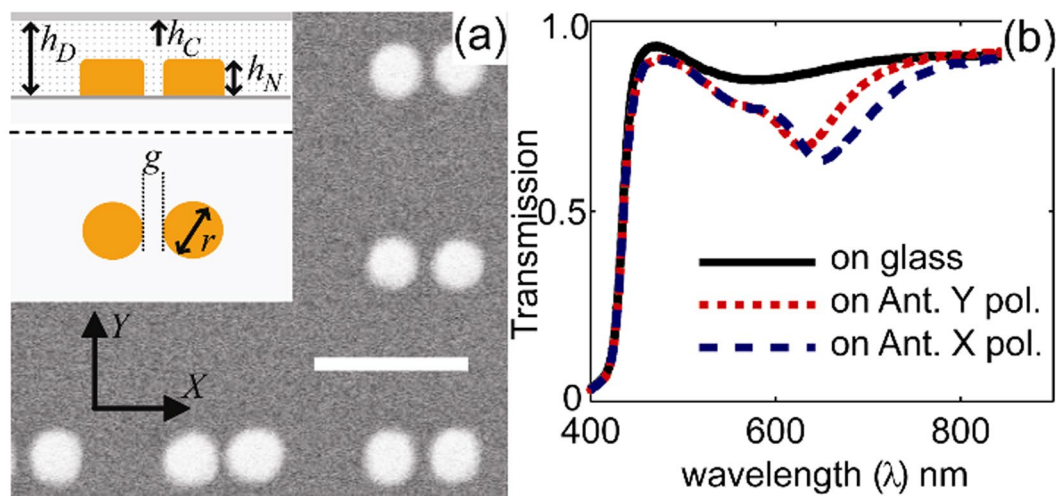
Figure 1. (a) A schematic, $h_D, h_N, h_C, g, r = 175, 60, 20, 14, 66$ nm respectively, and SEM image of the gold nanoantenna structure.

measured effective nonlinear refractive index, n_2, is enhanced by a factor of 140 relative to a BDPAS layer of the same thickness. This is achieved with only 3.7% of gold volume fraction. The numerical simulations show that only 60 nm (the nanoantenna's height) out of 175 nm of the BDPAS layer participates in the enhancement. Thus, the realistic enhancement of both the n_2 and α_2 is almost $3\times$ larger.

Results and Discussions

BDPAS has a strong one-photon absorption cross-section, 2.0×10^{-16} cm^2, at 390 nm[27], and negligible linear absorption in the visible. BDPAS has 42 π-conjugated bonds and exhibits strong 2PA from 600 nm to 800 nm, with a peak 2PA cross section of $\delta = 320$ GM (1 GM $= 10^{-50}$ cm^{4}s/photon) in dichloromethane (DCM) at 670 nm[27,28]. The dimensions of the gold nanoantennas shown in Fig. 1(a) (66 nm diameter, 60 nm height (including the 5 nm Ti layer), an antenna gap of 14 nm, and with an array periodicity of 250 nm) were designed so that the resonance wavelength (λ_r) is close to the 2PA cross section peak of BDPAS.

We demonstrate 2PA enhancement using an array of gold nanoantennas on an indium-tin-oxide (ITO) coated glass substrate coated with a layer of BDPAS by the thermal evaporation in a vacuum chamber. Since the localized field enhancement caused by nanoantennas typically has a range on the order of the nanoantenna thickness, a thin BDPAS film is sufficient to take advantage of nanoantenna enhancement. Our simulations show that 60 nm thickness is enough for the geometry used. The gold nanoantennas are fabricated using electron-beam lithography, as described in the Methods section, to produce larger grain sizes and a lower loss factor, resulting in a stronger plasmonic resonance and larger local electromagnetic fields[29]. A 175 nm BDPAS film with large molecular density of $N = 1.4 \times 10^{21}$ cm^{-3} [30], is covered using the thermal evaporation method by a 20 nm layer of silica to protect the sample. The linear refractive index of the BDPAS film is approximately $n_0 = 1.8$ at wavelengths longer than $\lambda = 500$ nm, as determined by spectroscopic ellipsometry. Figure 1(b) shows transmission spectra for the BDPAS film, and the film on nanoantennas at both the primary resonance polarization (X) with the incident E-field across the gap, and for the secondary polarization (Y). The transmission spectra show that the resonance wavelength, λ_r, of these gold nanoantennas coated with a BDPAS film is 665 nm for X polarization and 630 nm for Y polarization.

Open- and closed-aperture Z-scan measurements were used to measure the film's nonlinear index of refraction (n_2) and the nonlinear absorption coefficient (α_2) for the primary X polarization (see Methods section). Introduction of the nanoantennas in the BDPAS film results in a noticeable contribution of the nonlinear reflection in the nonlinear transmission. We show below that the effect of reflection can be taken into account using the n_2 obtained from the closed-aperture Z-scan in transmission. Relative to the usual method[31], we take into account transmission through the interfaces of the nonlinear slab to retrieve α_2 from the experimental results shown in Fig. 2a. Note that interface transmission does not change the wave phase, thus n_2 is retrieved in the usual way[31]. The BDPAS film and film on nanoantennas (indicated herein using subscripts F and N respectively) were measured at 600 nm and 650 nm. The strong nanoantenna resonance near 650 nm caused damage at an energy per pulse smaller than ~1 nJ (2 GW/cm^2) and did not provide usable data. Increasing the thickness of the top silica layer might be sufficient to increase the damage threshold of the nanoantennas, but further experiments are necessary to verify this.

Closed-aperture Z-scans at 600 and 700 nm, normalized by open-aperture scans, were used to measure the n_2 of an 11 mM solution of BDPAS in DCM in a 1 mm cuvette at 40 nJ (41 GW/cm^2), resulting in ($n_{2(BDPAS + DCM)}$ $(600) = 4.5 \pm 0.6 \times 10^{-16}$ cm^2/W) and ($n_{2(DCM)}(600) = 7.0 \pm 1.0 \times 10^{-16}$ cm^2/W). By normalizing the closed-aperture data for BDPAS in DCM by the data for pure DCM, we calculate ($n_{2(BDPAS)}(600) = -2.4 \pm 0.8 \times 10^{-16}$ cm^2/W) and ($n_{2(BDPAS)}(700) = 2.2 \pm 0.8 \times 10^{-16}$ cm^2/W) for 11 mM of BDPAS. Note that we assume the n_2 of DCM to be dispersionless across this wavelength range. This results in refractive cross-sections ($\delta_r = n_2 \hbar \omega k / N$) given in units of Göppert-Mayer[32] of $\delta_{r(BDPAS)}(600) = -1.3 \pm 0.4 \times 10^2$ GM and $\delta_{r(BDPAS)}(700) = 1.2 \pm 0.4 \times 10^2$ GM.
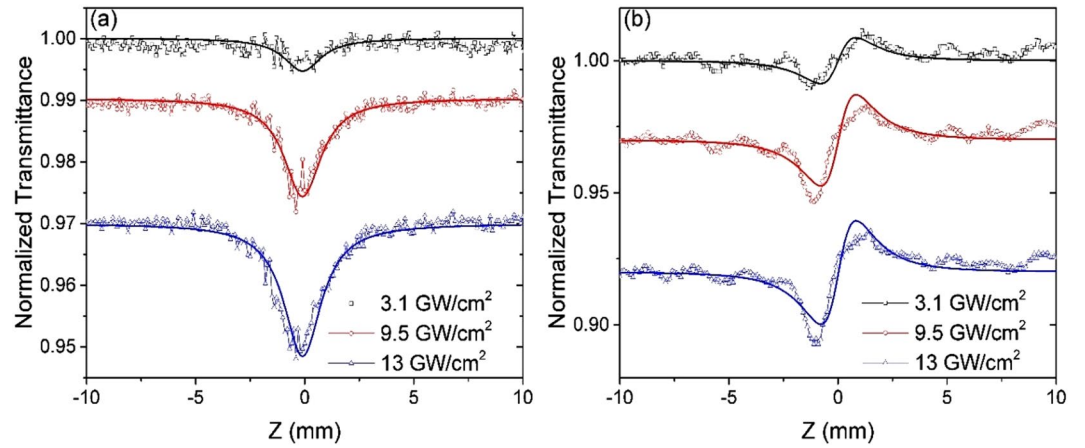
Figure 2. Z-scan data for 175 nm BDPAS film on nanoantennas sample [linear transmission offset for clarity]. (**a**) open-aperture with $\alpha_{2N}(600) = 300$ cm/GW fit, implying no nonlinear reflection, at 1.4, 4.3, and 6 nJ, and (**b**) Closed-aperture normalized by 1 mm glass, with $n_{2N}(600) = (0.7 \pm 0.2) \times 10^{-11}$ cm²/W fits, at 1.4, 4.3, and 6 nJ.

The n_2 at 600 nm for a sample including both the BDPAS film on nanoantennas and 1 mm glass substrate is retrieved using peak to valley transmission:

$$\Delta T_{p-v} = 0.406(1 - 0.4)^{0.25} \frac{2\pi}{\lambda\sqrt{2}} I_0 \left(n_{2\text{glass}} h_{\text{glass}} + n_{2N} h_N \frac{1 - \exp(-\alpha_N h_N)}{\alpha_N h_N} \right) \tag{1}$$

From Fig. 2b $\Delta T_{p-v} = 0.0375$ at 9.5 GW/cm², an effective nanoantenna length of $h_N \cdot 0.83$ and $n_{2(\text{glass})} = 3.0 \times 10^{-16}$ cm²/W[33]. Thus we obtain an n_2 for the 175 nm BDPAS film with nanoantennas layer of $n_{2N} = (0.7 \pm 0.2) \times 10^{-11}$ cm²/W, see Fig. 2(b), resulting in $\delta_{rN}(600) = 1.8 \times 10^4$ GM.

There was no detectable transmission change for the BDPAS film without nanoantennas.

Based on the known molecular density[30], and the refractive cross-section for BDPAS, $\delta_{r\,(\text{BDPAS})}(600)$, measured above, we give the nonlinear index of refraction of the film as $n_{2F}(600) \approx -5.0 \pm 1.4 \times 10^{-14}$ cm²/W and $n_{2F}(700) \approx 4.5 \pm 1.4 \times 10^{-14}$ cm²/W.

Using open-aperture Z-scans, shown in Fig. 2(a), we retrieve the nonlinear imaginary refractive index and consequently nonlinear absorption coefficient. The effect of reflection is taken into account using n_2 obtained from the closed-aperture Z-scan in transmission. Since the interface transmission does not change the wave phase, n_2 is retrieved in the usual way[31]. Relative to the usual method[31], the transmission through the interfaces of the nonlinear slab is taken into account to retrieve α_2 from the experimental results shown in Fig. 2a.

For intensity dependent transmission we take into account the reduced intensity at the second interface. Namely $T = T_1(I)A(I_{\text{eff}})T_2(Ie^{-\alpha h})$, where transmission at the first interface, transmission through the slab, and transmission at the second interface are: $T_{1,2} = 1 - R_{1,2} = 4n_{1,3}n/[(n_{1,3} + n)^2 + \kappa^2]$, $A = e^{-\alpha h}$, $n + i\kappa = n_{slab}$, $\alpha = 4\pi\kappa/\lambda$. The nonlinear change in transmission, taking into account the averaging coefficient $2^{3/2}$, is given by (see supplementary information for details):

$$2^{3/2}\frac{\Delta T}{T\,\Delta I} = -\frac{1}{n}\frac{(n^2 - n_1^2 - \kappa^2)}{(n_1 + n)^2 + \kappa^2}n_{\text{nl}} + \frac{n(n_1/n + 1)^2 + \kappa^2/n - 2\kappa}{(n_1 + n)^2 + \kappa^2}\kappa_{\text{nl}} -$$
$$-\frac{4\pi h}{\lambda}\kappa_{\text{nl}}\frac{1 - e^{-\alpha h}}{\alpha h} - \frac{1}{n}\frac{(n^2 - n_3^2 - \kappa^2)}{(n_3 + n)^2 + \kappa^2}n_{\text{nl}}e^{-\alpha h} + \frac{n(n_3/n + 1)^2 + \kappa^2/n - 2\kappa}{(n_3 + n)^2 + \kappa^2}\kappa_{\text{nl}}e^{-\alpha h}. \tag{2}$$

Using $n_{\text{nl}} = n_{2N} = 0.7 \times 10^{-11}$ cm²/W, $n_1 = 1.8$, $n_3 = 1.5$, from the linear reflection and transmission fitting $n = 2.3 + n_{\text{nl}}I$, $k = 0.117 + \kappa_{\text{nl}}I$ at $h = 175$ nm, and $T_{\text{exp}} \approx 0.6$, $\Delta T/T = 0.022$ at $\Delta I = 13$ GW/cm², we obtain $\kappa_{2N} = \kappa_{\text{nl}} = 0.17 \times 10^{-11}$ cm²/W and $\alpha_{2N} = \alpha_{\text{nl}} = 360$ cm/GW.

Note that, taking into account both absorption and reflection in the open-aperture transmission in Fig. 2a, the analysis gives $\alpha_{2N} = 360$ cm/GW instead of $\alpha_{2N} = 300$ cm/GW as given by the usual fitting procedure. Figure 3 shows the transmittance change (ΔT) versus irradiance retrieved from the open-aperture Z-scan results. Note that the nonlinear coefficients are calculated for an effective composite layer of BDPAS and nanoantennas. In the obtained results, the thickness of the effective composite layer is taken as the total thickness of BDPAS and nanoantennas. Another reasonable approach is to consider the effective layer thickness equal to the nanoantennas thickness, 60 nm, since the field enhancement is strong near the nanoparticles.

Our simulations below confirm that this second approach, with an effective thickness of 60 nm, better describes the experimental situation. Indeed, the intensity mapping in Fig. 4 shows that a layer of 60 nm contains the most intense local field. Also, using the simulated intensity-dependent transmission and reflection shown in Fig. 5, we find that nonlinear changes in transmission and reflection do not grow significantly with the thickness after 60 nm, see Fig. 6. Specifically, in this case, $n_{\text{nl}} = n_{2N} = 2.48 \times 10^{-11}$ cm²/W, $n_1 = 1.8$,
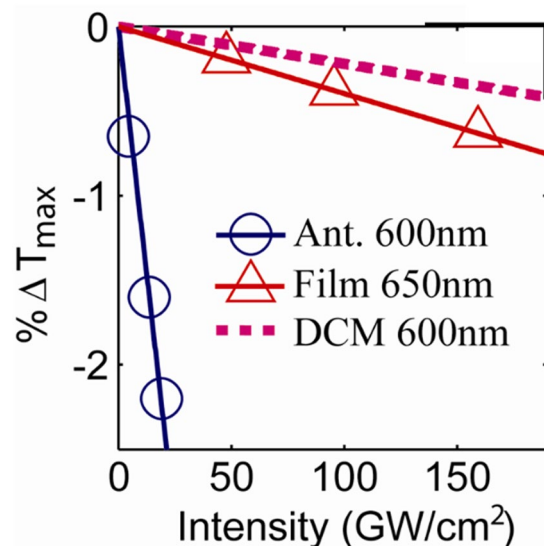
Figure 3. %ΔT from Z-scans vs. incident intensity for BDPAS with nanoantennas, BDPAS film, and BDPAS solution with exponential fit.
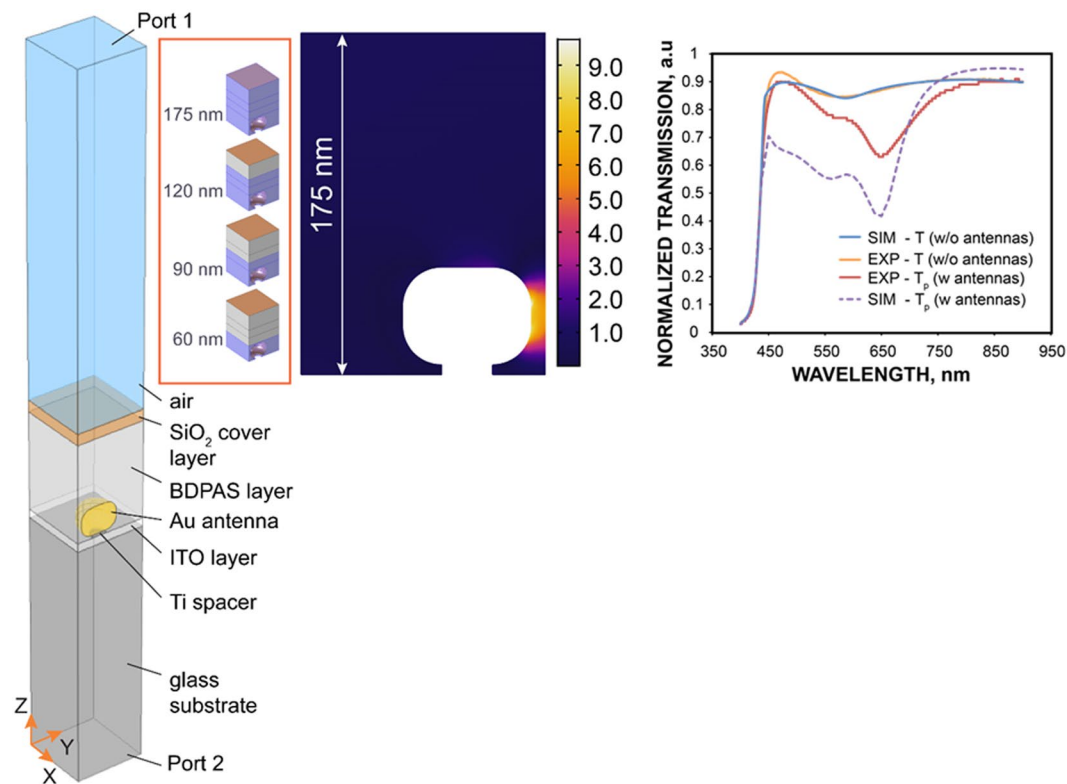

Figure 4. Unit cell of the FEM simulations (left), a distribution of the intensity in arbitrary units (center) at 600 nm, normalized transmission spectra with and without Au nanoantennas from the experiments and simulations (right). Simulations for BDPAS film use Eq. 3.

$n_3 = 1.5$, from linear reflection and transmission fitting $n = 2.4 + n_{nl}I$, $k = 0.31 + \kappa_{nl}I$ at $h = 60$ nm, and we obtain $\kappa_{2N} = \kappa_{nl} = 0.6 \times 10^{-11}$ cm^2/W and $\alpha_{2N} = \alpha_{nl} = 1257$ cm/GW.

We obtain $\alpha_{2F}(650) = 13$ cm/GW for the BDPAS film, and $\alpha_{2N}(600) = 360$ cm/GW for the BDPAS film with nanoantennas. The smaller 2PA of BDPAS at 600 nm ($\delta \approx 130$ GM in DCM) did not provide detectable attenuation to measure $\alpha_{2F}(600 \text{ nm})$.

From the measured $\alpha_{2F}(650)$, the 2PA cross-section of BDPAS in film form is calculated to be $\delta_F(650) = 287$ GM with ± 15% experimental error, which is in good agreement with that of BDPAS in DCM solution. Using the
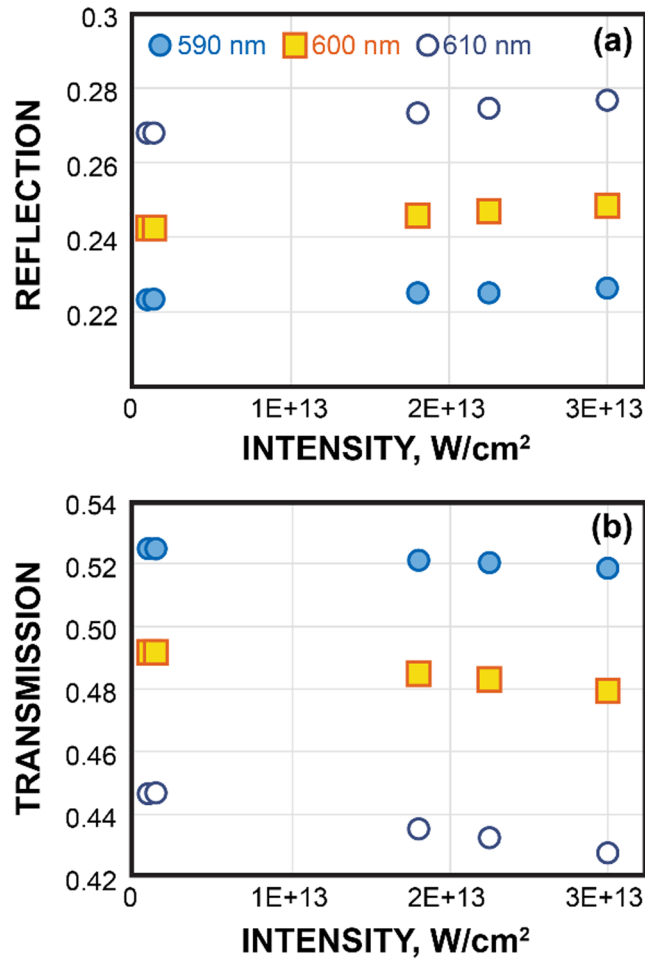
Figure 5. Intensity dependence of the reflection (**a**) and transmission (**b**) of the BDPAS with nanoantennas at wavelength 590, 600, and 610 nm.

wavelength dependence from ref.[27] results in an estimated $\delta_F(600) = 162$ GM, and using $\delta = (hc/\lambda)\,(\alpha_2/N)$ we obtain $\alpha_{2F}(600 \text{ nm}) = 6.8$ cm/GW for the 175 nm BDPAS film. Using $\mathrm{Re}[\chi^{(3)}] = n_2 \cdot (4/3)n_0^2\varepsilon_0 c$ and $\mathrm{Im}\chi^{(3)} = \alpha_2 \cdot (2n_0^2\varepsilon_0 c^2/3\omega)$, we obtain $\chi_N^{(3)}(600) = (8.1 + i1.9) \times 10^{-18}\mathrm{m}^2/V^2$ for BDPAS on the nanoantennas, and $\chi_F^{(3)}(600) = (-5.8 + i3.6) \times 10^{-20}\mathrm{m}^2/V^2$ and $\chi_F^{(3)}(700) = (5.3 + i12.7) \times 10^{-20}\mathrm{m}^2/V^2$ for the BDPAS film.

The analysis of matching FEM electromagnetic simulations of the nanoantenna-dye unit-cell from Fig. 1(a) supports the experiments as described below. The geometric dimensions and Au loss factor were fit to the experimental results using an efficient simplified model described in ref.[34]. The experimental geometry was simulated with a commercial full wave electromagnetic simulation software (Comsol Multiphysics) built on the finite-element method. The one-quarter unit cell of the sample bounded by the symmetry planes is shown in Fig. 4 (left). The BDPAS layer was composed of two sublayers, nonlinear and linear. The total thickness is always 175 nm, while the nonlinear one was changed as 10, 30, 60, 90, 120, and 175 nm to find an optimal thickness of the nonlinear material coating. The intensity distribution in Fig. 4 (center) shows that the maximum nonlinear change of the refractive index is expected in the gap in correspondence with the local field distribution and the BDPAS nonlinear refractive index. Figure 4 (right) illustrates the very good correspondence of the experimental and simulated spectra of the BDPAS and a relatively good shape correspondence of the BDPAS with Au nanoantennas. The discrepancy may be due to defects in the array fabrication (missing particles in nanoantennas).

The BDPAS linear permittivity was modeled by a Tauc-Lorentz term and two Lorentz oscillators,

$$\varepsilon_{\mathrm{BDPAS}} = \varepsilon_{\mathrm{TL}} + \sum_{j=1}^{2}\varepsilon_{L,j}. \tag{3}$$

A complete description of the Lorentz and Tauc-Lorentz terms along with their experimentally fitted coefficients are shown in the Supporting Information.

The refractive index inside a nonlinear host is,
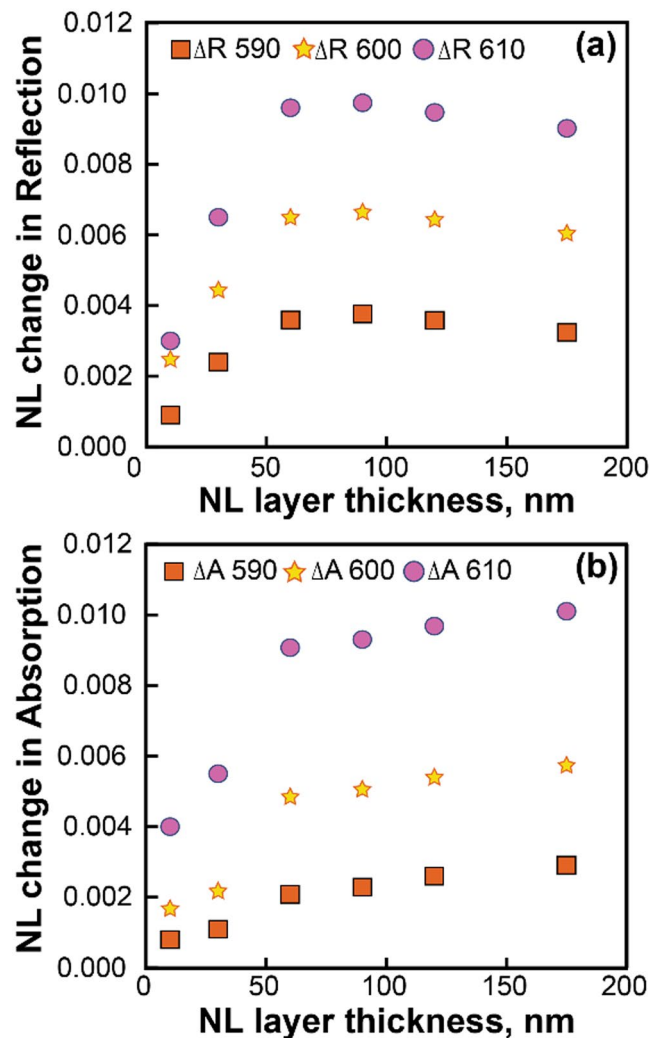
Figure 6. Change in absorption and reflection versus nonlinear layer (BDPAS) thickness with nanoantennas at wavelength 590, 600, and 610 nm.

$$n = n_0 + \left(n_2 + i\frac{\alpha_2}{2k_0}\right)I, \tag{4}$$

where $k_0 = 2\pi/\lambda$ is a free-space wave number, and inside a NL medium the intensities and the field magnitudes are linked as,

$$I = \frac{1}{2}\varepsilon_0 n'_0 c |E|^2, \qquad E(t) = \mathrm{Re}E\exp(-i\omega t), \tag{5}$$

with n'_0 being the real part of the linear component of refractive index.

In the FEM model, the nonlinear properties of the bulk film BDPAS have been taken into account by using $n_2 = -5.0 \times 10^{-18}\,\mathrm{m^2/W}$ and $\alpha_2 = 6.7 \times 10^{-11}\,\mathrm{m/W}$, while the real and imaginary parts of $\chi^{(3)}$ were computed as

$$\mathrm{Re}[\chi^{(3)}] = \frac{4}{3}\varepsilon_0 c n'^2_0 n_2 \tag{6}$$

$$\mathrm{Im}[\chi^{(3)}] = \frac{2}{3}\varepsilon_0 c n'^2_0 \alpha_2/k_0 \tag{7}$$

with the principal components of the anisotropic dielectric function in the medium defined as,

$$\varepsilon_{ii} = n_0^2 + \frac{3}{4}\chi_{ii}^{(3)}|E_i|^2 i \in \{x, y, z\} \tag{8}$$

	$n_2(600)$, $\times 10^{-18} \mathrm{m^2/W}$	$\alpha_2(600)$, $\times 10^{-11}\mathrm{m/W}$	$\chi^{(3)}(600)$, $\times 10^{-20}\mathrm{m^2/V^2}$	$\frac{n_{2N}}{n_{2F}}$	$\frac{\alpha_{2N}}{\alpha_{2F}}$
BDPAS Film	−5	6.8	$-5.8 + i3.6$		
BDPAS with NAs Exp (175 nm)	700	360	$812 + i190$	−140	53
BDPAS with NAs Sim (175 nm)	620	240	$720 + i37$	−125	36
BDPAS with NAs Sim (60 nm + 115 nm)	700	1100	$810 + i580$	−140	160

Table 1. Summary of experimental and simulation results.

The solution of resulting nonlinear wave equation $\nabla \times \nabla \times \mathrm{E} - k_0\, \varepsilon\, \mathrm{E} = 0$ in the entire domain is obtained self-consistently at each excitation step with the commercial FEM solver (COMSOL Multiphysics, Wave Optics Module) using a high-performance iterative method (double dogleg). We should note that to avoid possible numerical issues and speed up simulations the illumination intensity is taken to be gradually increasing with the previous solution used as a seed for a new step.

From the literature[35,36] for "fast" nonlinearity we take $\chi_{\mathrm{Au}}^{(3)} = (-1.1 + i1.0) \times 10^{-22}\ \mathrm{m^2/V^2} \ll \chi_{\mathrm{BDPAS}}^{(3)}$. The simulated intensity dependent transmission and reflection coefficients are shown in Fig. 5.

The thickness dependence (Fig. 6) shows that the nonlinear response is almost saturated after 60 nm. The nonlinear transmission and reflection obtained with the full wave simulations were then fitted with the variable complex refractive index $N = n + ik$ mimicking the intensity dependence. This is done with the J. A. Wollam software[37,38]. All the layers are glass 1 mm ($n = 1.52$) without backside reflection, ITO 15 nm ($n = 1.9586$), BDPAS 175 nm, SiO$_2$ 20 nm ($n = 1.458$). The fitted refractive index corresponds to the BDPAS parameters without nanoantennas and to the effective nonlinear refractive index and effective nonlinear absorption of the effective uniform layer in case of the BDPAS with nanoantennas. Thus for 175 nm BDPAS film we get at 600 nm:

$$n = 1.8 - 16 \times 10^{-4}(I/I_{\mathrm{nl}}),\ \ k = 0.00537 + 9.3 \times 10^{-4}(I/I_{\mathrm{nl}}),\ \ \text{where}\, I_{\mathrm{nl}} = 3 \times 10^{14}\ \frac{W}{m^2}.$$

This retrieval procedure via the fitting gives for the BDPAS $n_{2F}(600) = -16 \times 10^{-4}/I_{\mathrm{nl}} = -5.3 \times 10^{-18}\ \mathrm{m^2/W}$, $\kappa_2 = 9.3 \times 10^{-4}/I_{\mathrm{nl}} = 3.1 \times 10^{-18}$, and $\alpha_{2F}(600) = 2k_0\kappa_2 = 6.5 \times 10^{-11}$ m/W. This provides a control retrieval result matching the accepted starting parameters of the BDPAS layer.

The BDPAS with Au nanoantennas and effective layer thickness L = 175 nm at 600 nm results in: $n = 2.3 + 0.018(I/I_{\mathrm{nl}})$, $k = 0.117 + 0.0033(I/I_{\mathrm{nl}})$, where $I_{\mathrm{nl}} = 2.9 \times 10^{13}\ W/m^2$. Thus at 175 nm for the effective uniform layer $n_{2\mathrm{eff}}(600) = 0.62 \times 10^{-11}\ \mathrm{cm^2/W}$, $\alpha_{2\mathrm{eff}}(600) = 240$ cm/GW. Experimental results give $n_{2N} = (0.7 \pm 0.2) \times 10^{-11}\ \mathrm{cm^2/W}$, $\alpha_{2N} = 360$ cm/GW.

Since approximately only the first 60 nm near the nanoantennas contribute to the enhancement (see Fig. 6), it makes sense to retrieve the complex nonlinear refractive index for the composition of 60 nm of the effective nonlinear BDPAS/Au nanoantennas hybrid and keep the remaining 115 nm as a linear layer. The retrieved effective refractive index for the 60 nm uniform effective layer is: $n = 2.4 + 0.021(I/I_{nl})$, $k = 0.31 + 0.015(I/I_{nl})$, where $I_{\mathrm{nl}} = 2.9 \times 10^{13}\ W/m^2$. Correspondingly, this gives for the 60 nm effective layer $n_{2\mathrm{eff}}(600) = 0.7 \times 10^{-11}\ \mathrm{cm^2/W}$, $\alpha_{2\mathrm{eff}}(600) = 1100$ cm/GW.

We also evaluate another approach to define an effective third-order susceptibility, $\chi_{\mathrm{eff}}^{(3)}$, widely used in the earlier literature[25] and recent developments[5]. Namely $\chi_{\mathrm{eff}}^{(3)}$ is defined as Eq. 9, where $f, g^{(3)}$ are the volume filling fraction and enhancement factor respectively, subscripts {h, in} denote the host (dye) and inclusions (gold).

$$X_{\mathrm{eff}}^{(3)} = f_{\mathrm{in}} g_{\mathrm{in}}^{(3)} \chi_{\mathrm{in}}^{(3)} + f_{\mathrm{h}} g_{\mathrm{h}}^{(3)} \chi_{\mathrm{h}}^{(3)} \tag{9}$$

The E-field extracted from simulations was used to find the complex nonlinear enhancement ($g_{\mathrm{h}}^{(3)}$), $f_{\mathrm{h}} = 0.964$ from the above geometry since $X_{\mathrm{eff}}^{(3)}$ in our system is dominated by the host (BDPAS) term. One should mention that the approximation based on the local field factor is not practical as this follows from our evaluation in the supplementary information. We conclude that local field enhancement is strongly intensity dependent and cannot be used to define the effective nonlinear susceptibilities. Any detectable nonlinearity will make the approximation used in the literature[5,25] unacceptable.

Table 1 summarizes the experimental and simulations' results. The final enhancement of the nonlinear susceptibility of the dye due to the nanoantennas is found by comparing both the experimental results ($\chi_{\mathrm{N}}^{(3)}$) and the FEM simulations ($X_{\mathrm{eff}}^{(3)}$) of the composite structure to the BDPAS film ($\chi_{\mathrm{F}}^{(3)}$).

The nonlinear refractive index of the BDPAS layer is enhanced by $n_{2N}/n_{2F} = -140$x from experiment, and $n_{2\mathrm{Neff}}/n_{2F} = -125$x from simulations at 600 nm. The retrieval using the effective thickness 60 nm, which corresponds to the characteristic thickness of the nonlinear response saturation presented in Fig. 6, gives $n_{2\mathrm{Neff}}/n_{2F} = -140$. While the sign change in n_2 is reproduced in both cases, the magnitude deviation is most likely due to the difference in the resonance quality between the experimental sample and simulated unit cell, which is seen for the linear response in Fig. 1b. The 2PA of the dye layer is enhanced by $\alpha_{2N}/\alpha_{2F} = 53$ times in the experiment, and $\alpha_{2\mathrm{Neff}}/\alpha_{2F} = 36$ times from simulations at 600 nm. Note that the enhancement due to the nanoantennas changes the sign of the nonlinear refractive index. Such a complex enhancement of the local field in a composite medium has been discussed earlier[39]. The main reason for the imaginary part of the local field enhancement is the phase shift between the local field and applied field. It is also important that the local field varies in both, magnitude and phase with coordinates near the nanoantenna particles. The simulations suggest also that the

nonlinear changes in transmission have a contribution from both nonlinear changes in reflection and in absorption. However, the Z-scan data for n_2 allows separating the effects of absorption to get α_2 as was shown above.

Conclusions

Gold dipole nanoantennas that produce strong local electromagnetic fields were used to enhance both the nonlinear refractive index and 2PA of a nonlinear dye. Bi-periodic gold nanoantenna arrays with nonlinear dyes also have a large wavelength dependent theoretical enhancement as has been shown from simulations. Furthermore, experimental results have shown that the nonlinear refractive index is enhanced by $140\times$ with a sign change from negative to positive and a $53\times$ enhancement in nonlinear (2PA) absorption at $\lambda = 600$ nm for BDPAS (4,4′-bis(diphenylamino)stilbene) with only 10% of surface coverage or 3.7% volume fraction of the gold nanoantennas. Since only 60 nm out of 175 nm of the BDPAS layer contributes to the enhancement, the realistic enhancement of both the n_2 and α_2 is ~3 times larger.

Both real and imaginary parts of the BDPAS $\chi_F^{(3)}$ contribute to the effective nonlinear absorption of the BDPAS/Au nanoantenna composite material, due to the complex nature of the enhancement factor resulting in the sign flip for the nonlinear refractive index. This fact, along with the tunable enhancement of the plasmon resonance, makes it possible to control the effective nonlinear response of the composite film. The above results demonstrate that the nonlinear composite can be further optimized through appropriate selection of component materials.

Methods

The gold nanoantennas are fabricated using electron-beam lithography on an ITO-coated glass substrate with a 15 nm ITO layer. An electron-beam evaporator is used to produce a 5 nm adhesion layer of titanium followed by a 55 nm gold film with a 1 Å/s deposition rate in a 7×10^{-7} Torr vacuum chamber (Airco). After lift-off the nanoantennas are annealed at 400 °C for 2 minutes by a rapid thermal processing system (RTP, Minipulse RTA), which has been shown to produce larger grain sizes and a lower loss factor, resulting in a stronger plasmonic resonance and larger local electromagnetic fields[29]. A 175 nm BDPAS film was then deposited using thermal evaporation in a vacuum chamber, followed by a 20 nm layer of silica to protect the sample. The linear refractive index of the BDPAS film is determined by spectroscopic ellipsometry, which is approximately $n_0 = 1.8$ at wavelengths longer than $\lambda = 500$ nm. Open- and closed-aperture Z-scan measurements were used to measure the film's nonlinear index of refraction (n_2) and the nonlinear absorption coefficient (α_2) for the primary X polarization. The effect of reflection can be taken into account using the n_2 obtained from the closed-aperture Z-scan in transmission. Relative to the usual method[31], we take into account transmission through the interfaces of the nonlinear slab to retrieve α_2 from the experimental results as explained in supplementary information. Note that interface transmission does not change the wave phase, thus n_2 is retrieved in the usual way[31]. A femtosecond optical parametric amplifier, OPA (Light Conversion, TOPAS-800), pumped by a Ti:Sapphire regenerative amplifier laser system (Clark MXR, CPA 2010), with a pulse duration of 140 fs (FHWM), 1 kHz repetition rate, was used. The focused spot size varied for different measurements, so both pulse energy and irradiance are provided.

References

1. Su, K. H. *et al.* Interparticle Coupling Effects on Plasmon Resonances of Nanogold Particles. *Nano Lett.* **3**(8), 1087–1090 (2003).
2. Kim, S. *et al.* High-harmonic generation by resonant plasmon field enhancement. *Nature* **453**, 757–760 (2008).
3. Bakker, R. M. *et al.* Nanoantenna array-induced fluorescence enhancement and reduced lifetimes. *New J. Phys.* **10**, 125022–16 (2008).
4. Glass, A. M. *et al.* Enhanced two-photon fluorescence of molecules adsorbed on silver particle films. *Phys. Rev. B: Condens. Matter* **24**, 4906 (1981).
5. Kohlgraf-Owens, D. C. & Kik, P. G. Structural control of nonlinear optical absorption and refraction in dense metal nanoparticle arrays. *Opt. Express* **17**, 15032–15042 (2009).
6. Wenseleers, W. *et al.* Five Orders-of-Magnitude Enhancement of Two-Photon Absorption for Dyes on Silver Nanoparticle Fractal Clusters. *J. Phys. Chem. B* **106**, 6853–6863 (2002).
7. Cohanoschi, I. & Hernandez, F. E. Surface Plasmon Enhancement of Two- and Three-Photon Absorption of Hoechst 33 258 Dye in Activated Gold Colloid Solution. *J. Phys. Chem. B* **109**, 14506–14512 (2005).
8. Cohanoschi, I., Yao, I. S., Belfield, K. D. & Hernández, F. E. Effect of the concentration of organic dyes on their surface plasmon enhanced two-photon absorption cross section using activated Au nanoparticles. *J. Appl. Phys.* **101**, 086112–3 (2007).
9. Hache, F., Ricard, D. & Flytzanis, C. Optical nonlinearities of small metal particles: Surface-mediated resonance and quantum size effects. *J. Opt. Soc. Am. B* **3**, 1647–1655 (1986).
10. Bloemer, M. J., Haus, J. W. & Ashley, P. R. Degenerate four-wave mixing in colloidal gold as a function of particle size. *J. Opt. Soc. Am. B* **7**, 790–795 (1990).
11. Uchida, K. *et al.* Optical nonlinearities of a high concentration of small metal particles dispersed in glass: copper and silver particles. *J. Opt. Soc. Am. B* **11**, 1236–1243 (1994).
12. Rautian, S. G. Nonlinear spectroscopy of the degenerate electron gas in spherical metallic particles. *SoV. Phys. JETP* **85**, 451–461 (1997).
13. Drachev, V. P., Buin, A. K., Nakotte, H. & Shalaev, V. M. Size Dependent χ(3) for Conduction Electrons in Ag Nanoparticles. *Nano Letters* **4**, 1535–1539 (2004).
14. Mai, H. H. *et al.* Nonlinear Optical Properties of Ag Nanoclusters and Nanoparticles Dispersed in a Glass Host. *J. Phys. Chem. C* **118**, 15995–16002 (2014).
15. Philip, R., Chantharasupawong, P., Qian, H., Jin, R. & Thomas, J. Evolution of Nonlinear Optical Properties: From Gold Atomic Clusters to Plasmonic Nanocrystals. *Nano Letters* **12**, 4661–4667 (2012).
16. Liberman, V., Sworin, M., Kingsborough, R. P., Geurtsen, G. P. & Rothschild, M. Nonlinear bleaching, absorption, and scattering of 532-nm-irradiated plasmonic nanoparticles. *J. Appl. Phys.* **113**, 053107–10 (2013).
17. Zhang, X., Luo, W., Wang, L.-J. & Jiang, W. Third-order nonlinear optical vitreous material derived from mesoporous silica incorporated with Au nanoparticles. *J. Mat Chem. C* **2**, 6966–6970 (2014).
18. Drachev, V. P., Perminov, S. V., Rautian, S. G., Safonov, V. P. & Khaliullin, E. N. Polarization effects in silver nano-aggregates caused by local and nonlocal nonlinear-optical responses. *J. of Experim. and Theor. Physics* **95**, 901–915 (2002).

19. Drachev, V. P., Perminov, S. V., Rautian, S. G. & Safonov, V. P. Giant nonlinear optical activity in aggregated silver nanocomposites. *JETP Letters* **68**, 651–656 (1998).
20. Shorokhov, A. S. *et al*. Ultrafast control of third-order optical nonlinearities in fishnet metamaterials. *Scientific Reports* **6**, 28440, https://doi.org/10.1038/srep28440 (2016).
21. Khurgin, J. B. & Sun, G. Plasmonic enhancement of the third order nonlinear optical phenomena: Figures of merit. *Opt. Express* **21**, 27460–27480 (2013).
22. Hasan, S. B., Lederer, F. & Rockstuhl, C. Nonlinear plasmonic antennas. *Materials Today* **7**, 478–485 (2014).
23. Valle, G. D. *et al*. Nonlinear anisotropic dielectric metasurfaces for ultrafast nanophotonics. *ACS Photonics* **4**, 2129–2136 (2017).
24. Debrus, S. *et al*. Z-scan determination of the third-order optical nonlinearity of gold: silica nanocomposites. *J. Appl. Phys.* **88**, 4469–4475 (2000).
25. Stroud, D. & Hui, P. M. Nonlinear susceptibilities of granular matter. *Phys. Rev. B: Condens. Matter* **37**, 8719–8724 (1988).
26. Ehrlich, J. E. *et al*. Two-photon absorption and broadband optical limiting with bis-donor stilbenes. *Opt. Lett.* **22**, 1843–1845 (1997).
27. Drobizhev, M., Rebane, A., Suo, Z. & Spangler, C. W. One-, two- and three-photon spectroscopy of [pi]-conjugated dendrimers: cooperative enhancement and coherent domains. *J. Lumin.* **111**, 291–305 (2005).
28. Makarov, N. S., Drobizhev, M. & Rebane, A. Two-photon absorption standards in the 550-1600 nm excitation wavelength range. *Opt. Express* **16**, 4029–4047 (2008).
29. Chen, K.-P., Drachev, V. P., Borneman, J. D., Kildishev, A. V. & Shalaev, V. M. Drude Relaxation Rate in Grained Gold Nanoantennas. *Nano Lett.* **10**, 916–922 (2010).
30. ChemBlink, "Online Database of Chemicals from Around the World: BDPAS" retrieved 4/3/2010, http://www.chemblink.com/products/202748-68-3.htm (2010).
31. Sheik-Bahae, M., Said, A. A., Wei, T. H., Hagan, D. J. & Van Stryland, E. W. Sensitive Measurement of Optical Nonlinearities Using a Single Beam. *Journal of Quantum Electronics QE* **26**, 760–769 (1989).
32. Balu, M. *et al*. Broadband Z-scan characterization using a high-spectral-irradiance, high-quality supercontinuum. *J. Opt. Soc. Am. B* **25**, 159–165 (2008).
33. Boyd, R. W. Nonlinear Optics. 3rd ed. Academic Press, Inc., SanDiego, 2008.
34. Borneman, J. D., Chen, K.-P., Kildishev, A. V. & Shalaev, V. M. Simplified model for periodic nanoantennae: linear model and inverse design. *Opt. Express* **17**, 11607–11617 (2009).
35. Ganeev, R. A., Ryasnyansky, A. I., Kamalov, S. R., Kodirov, M. K. & Usmanov, T. Nonlinear susceptibilities, absorption coefficients and refractive indices of colloidal metals. *J. Phys. D: Appl. Phys.* **34**, 1602–1611 (2001).
36. Mehendale, S. C. *et al*. Nonlinear refraction in aqueous colloidal gold. *Opt. Commun.* **133**, 273–276 (1997).
37. The simulations for the experimental and the effective, stratified, planar structures were performed with ellipsometry software (W-VASE, J. A. Woollam Co., Inc.) that is based on a 4x4 scattering-matrix method for solving Maxwell's Equations Ref. [38].
38. Azzam, R. M. A. & Bashara, N. M. Ellipsometry and polarized light. North Holland (1987).
39. Smith, D. D., Fischer, G., Boyd, R. W. & Gregory, D. A. Cancellation of photoinduced absorption in metal nanoparticle composites through a counterintuitive consequence of local field effects. *J. Opt. Soc. Am. B: Opt. Phys.* **14**, 1625–1631 (1997).

Acknowledgements

Author Contributions

Project planning: V.P.D., V.M.S., R.A.N., N.P., S.R.M., D.J.H., E.W.V.S.; sample preparation and structural characterization: K.-P.C. and J.D.B. under supervision V.P.D.; organic film synthesis and fabrication: S.R.M., K.Y., R.A.N.; numerical simulations and analysis: A.V.K. and V.P.D.; nonlinear measurements and analysis: L.A.P., S.W., T.R.E., D.J.H., E.W.V.S.; All authors contributed to overall data analysis and scientific discussions. V.P.D., A.V.K., J.D.B., L.A.P., D.J.H., E.W.V.S. wrote the manuscript with contributions from all authors.

Additional Information

Supplementary information accompanies this paper at https://doi.org/10.1038/s41598-017-19066-3.

Competing Interests: The authors declare that they have no competing interests.

Publisher's note: Springer Nature remains neutral with regard to jurisdictional claims in published maps and institutional affiliations.